Available online at www.sciencedirect.com

ScienceDirect

journal homepage: www.elsevier.com/locate/he

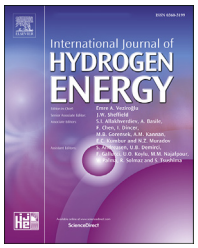

Morphology controlled synthesis of Pd_2Ge nanostructures and their shape-dependent catalytic properties for hydrogen evolution reaction

Jee-Yee Chen [1], *Shao-Lou Jheng* [1], *Cheng-Ying Chan*, *Hsing-Yu Tuan* [*]

Department of Chemical Engineering, National Tsing Hua University, Hsinchu 30013, Taiwan

ARTICLE INFO

Article history:
Received 15 December 2018
Received in revised form
28 February 2019
Accepted 7 March 2019
Available online 16 April 2019

Keywords:
Germanium
Palladium
Hydrogen evolution reaction
Nanomaterials
Shape dependent
Synthesis

ABSTRACT

Pd_2Ge with different shape-controlled morphologies were obtained via a one-pot hot injection method. Through investigating the effect of reaction conditions, including surfactants, reaction time and temperature, the shape of synthesized Pd_2Ge can be tuned from nanoparticles to nanorods and nanowires. These various nanostructures of Pd_2Ge enable an investigation and comparisons as electrocatalysts for hydrogen evolution reaction (HER). The results of catalyst activity indicate HER properties are shape-dependent. Compared with the nanostructures and commercial Pd black, the nanorods show more active than the commercial Pd black and other nanostructures. The nanorods display outstanding activity as electrocatalyst, and fascinating endurance remain still after 20,000 cycles CV swept and under a static overpotential of −0.5 V vs. RHE for 48 h. The better stability and activity performance of nanorods may be due to the exposed surface composed of two crystal facets, (111) and (110), which increase the active sites of the nanorods.

© 2019 Hydrogen Energy Publications LLC. Published by Elsevier Ltd. All rights reserved.

Introduction

An electrocatalytic hydrogen evolution reaction (HER) has garnered a significant amount of recognition as a clean and renewable energy. Platinum (Pt) [1–4] and palladium (Pd) [5–7] are two of the most generally used catalysts in HER. In Pd-based materials, the germanium (Ge)–Pd system shows its potential since Ge-based materials have excellent electronic characteristics. To that end, Ge–Pd materials have been widely investigated in different electronic applications [8–12]. Moreover, Ge–Pd is rich in binary phases (shown in Fig. S1) [13]. Among all the phases, Pd_2Ge is the most stable phase for its highest melting point and the large phase changing region. The high activity of Ge–Pd as a catalyst has been developed since the 1880s [14]. Back in the early 1990s, Bodnar et al. pointed out promotion of Pd with Ge which exhibited higher activity than noble metals. They systematically explored bulk Pd adsorption of Ge, and demonstrated the structure would affect adsorption's sensitivity [10]. Later, Gootzen et al. used a Pd electrode with Ge coating on the surface in the nitrate reduction [11]. In this research, they demonstrated the reduction of nitrate rate strongly enhanced the formation of the Ge–Pd alloy, and indicated the limited proportion of germanium in the alloy affected the performance. Only when the alloy proportion of germanium was above 0.2, the

* *Corresponding author.*
E-mail addresses: chen.8363@osu.edu (J.-Y. Chen), a1593577852@hotmail.com (S.-L. Jheng), hytuan@che.nthu.edu.tw (H.-Y. Tuan).
[1] These authors contributed equally to this work.
https://doi.org/10.1016/j.ijhydene.2019.03.062
0360-3199/© 2019 Hydrogen Energy Publications LLC. Published by Elsevier Ltd. All rights reserved.

enhanced effect would occur. However, only few examples of Ge–Pd materials applied as electrocatalysts were explored as nanostructures [15,16].

Nanoscale-morphological controlling has been investigated in correlations and effects between morphologies and catalytic, electronic, thermal, selective properties [17–21]. Solution-phase synthesis is commonly used on size, morphology and structure control for nanostructures via various reaction conditions. Nanoparticles may form in cubic or polyhedron structures with appropriate surfactants, reaction temperatures, or ligands [22–25]. In 2001, Biacchi et al. demonstrated monodisperse nanoparticles with several different morphologies via systematic control of temperature, polyol solvent, and precursors [25]. Numerous researchers have further carried out investigating the shape-dependent characteristics. As a catalyst, shape control is an important issue because exposed facets greatly affect the catalytic reaction results [26–28]. For example, Huang et al. systematically developed a shape evolution from cube to rhombic dodecahedron, and investigated the facet-effect of different structures [29]. The work of Cu_2O nanocrystals clearly demonstrated the synthesis process and effect of the reaction condition to the product morphologies. In the result, Cu_2O nanocrystals displayed enhanced photocatalytic and electrical conductivity performance because of the specific active facets exposed. Therefore, electrocatalytic performance could be enhanced by shape evolution.

Herein, for the first example, Pd_2Ge nanoparticles were synthesized by decomposition of germanium (IV) iodide (GeI_4) precursor and palladium (II) iodide (PdI_2) in the presence of a mixture of oleylamine (OLA), oleic acid (OA)), trioctylphosphine (TOP) and dodecanethiol under argon atmosphere at 260 °C–340 °C. Through systematically tuning reaction conditions, various shapes of the synthesized products were obtained with morphologies ranging from nanoparticle, nanowires, and nanorods. An investigation and comparisons of Pd_2Ge nanostructures as electrocatalysts for hydrogen evolution reactions were also carried out.

Results and discussions

Synthesis and characterization

Through injecting the GeI_4 solution into preheated PdI_2 solution in three-neck flask, which attached to a Schlenk line system with dynamic argon steam environment, Pd_2Ge nanostructures were synthesized. After removing the uncovered precursor by centrifugation, Pd_2Ge products were yielded (shown in Fig. 1). In the transmission electron microscopy (TEM) (shown in Fig. 1(a)), the synthesized products obtained two morphologies: nanorods and nanoparticles. The products were further characterized by X-ray diffraction (XRD), and the results were compared and interpreted with standard database (JCPDS card no. 31–0559).

Shown in Fig. 1(b), the main characteristic peaks appeared at 37.6°, 40.8°, and 46.9°, which respectively corresponded to (111), (201)/(210) and (300) crystal facets, indicating the sample was hexagonal structure. Also, no other impurities were detected by XRD and the XRD simulation corresponded to the experimental results (shown in Fig. 1(b)). The synthesized product was then analyzed by the energy dispersive spectrometer (EDS) (shown in Fig. 1 (c)). The percentage of Ge and Pd, from the EDS results (inserted in Fig. 1 (c)), were 34.8% and 65.2%, respectively, and the ratio of Ge to Pd was closed to 1:2.

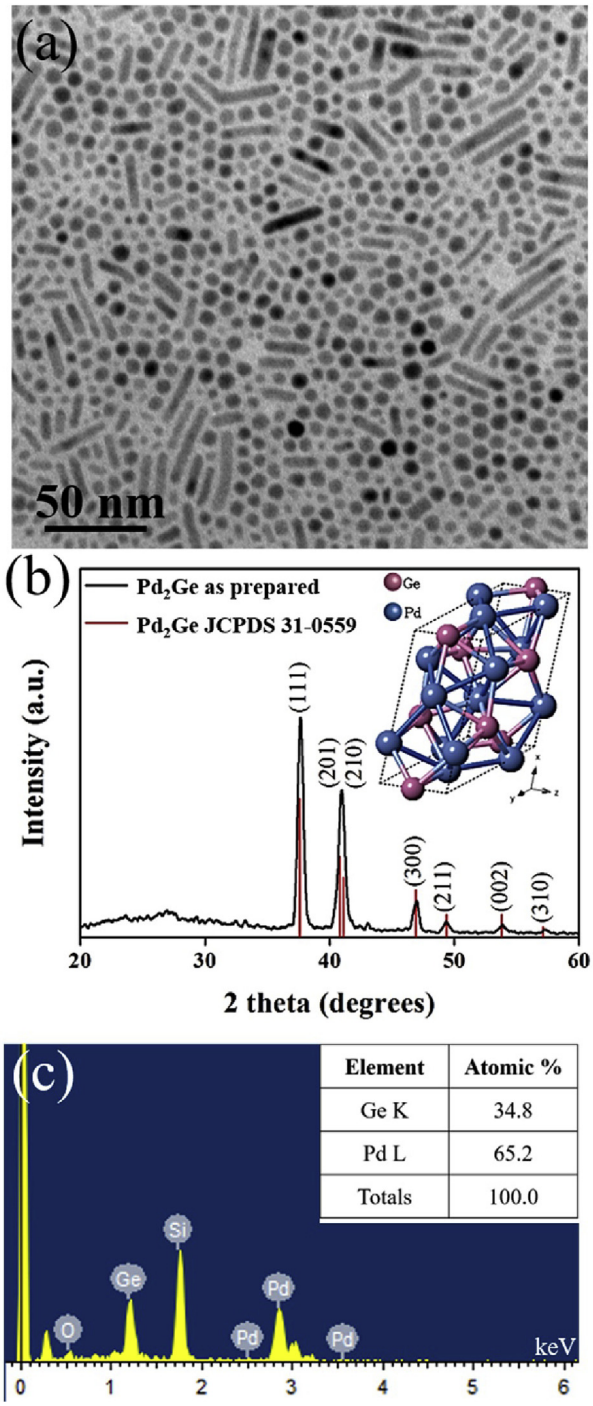

Fig. 1 – (a) TEM image, (b) XRD pattern with an insertion of the simulated hexagonal structure, (c) EDS result and the inserted is Ge to Pd atomic percentage table of Pd_2Ge nanoproducts.

Furthermore, the Pd_2Ge products were also examined with X-ray photoelectron spectroscopy (XPS) in order to understand the surface states. All the binding energies (displayed in Fig. 2(a–c)) have been corrected with C 1s (284.8 eV) reference (shown in Fig. 2 (a)). The regions of Ge 3d (shown in Fig. 2 (b)) and Pd 3d (shown in Fig. 2 (c)) were labelled. In the result of Ge, the peaks split to the element type (located at 29.4 eV, $3d_{5/2}$) and the valence +4 state type (located at 32.5 eV, $3d_{5/2}$) peaks, indicating the Pd_2Ge products would contained partially GeO_2 in the surface because of the exposure in air. The Pd 3d peaks illustrated the $3d_{3/2}$ and $3d_{5/2}$ of Pd metal with a separation located at 445.47 eV and 340.73 eV.

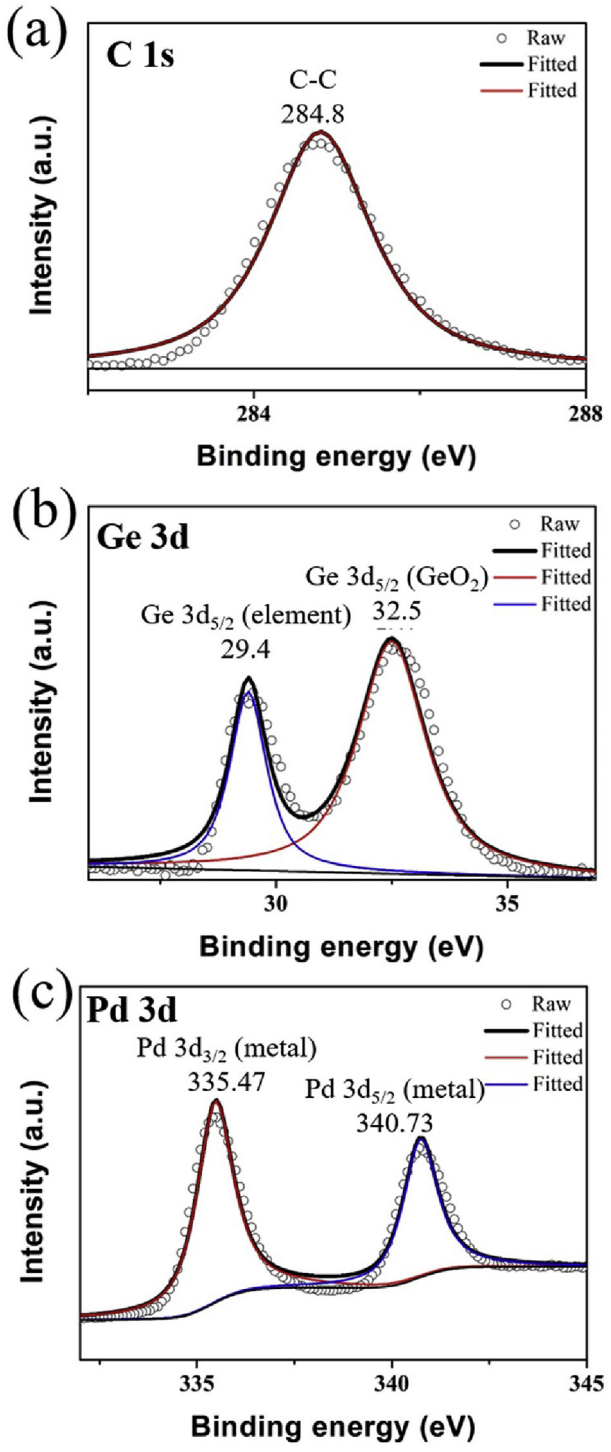

Fig. 2 – The XPS spectra of Pd_2Ge nanoparticles: (a) C 1s, (b) Ge 3d, and (c) Pd 3d.

Synthesis and characterization of Pd2Ge nanoparticles

Pd_2Ge nanoparticles were obtained by PdI_2 solution injected into GeI_4 in oleic acid (OA) and oleylamine (OLA) surfactants mixtures. The Pd_2Ge nanoparticles were explored through various electron microscopies, including scanning electron microscopy (SEM), TEM and high resolution transmission electron microscopy (HRTEM) for obtaining the detailed morphologies and structures. From Fig. 3(a and b), the SEM and TEM images revealed monodispersed spherical nanoparticles with an average diameter of 15 ± 5 nm. Further, from the HRTEM images (shown in Fig. 3(c and d)) and its fast Fourier transform (FFT) patterns of the nanoparticles (inserted in Fig. 3(d)), the detailed morphologies were achieved.

Synthesis and characterization of Pd2Ge nanorods

Pd_2Ge nanorods were synthesized via the similar method as nanoparticles but with PdI_2 dissolved in dodecanethiol solution at 300 °C. Shown in TEM and HRTEM images in Fig. 4(a–f), the low magnification TEM image (shown in Fig. 4(a)) displayed that the synthesized nanorods have an aspect ratio range of 2–16 (displayed in Fig. 4(b)). Detailed morphology can be seen in the TEM (shown in Fig. 4(c)) and HRTEM (shown in Fig. 4(d and f)). The selected area electron diffraction (SAED) image in Fig. 4(e) revealed the growing planes were (001), (111), (110) and (221). With the HRTEM image shown in Fig. 4(f), the surface of the nanorods was composited by two different crystal facets, (111) and (110), which increase the active sites of the nanorods in the HER.

Synthesis and characterization of Pd2Ge nanowires

Pd_2Ge nanowires were synthesized via similar synthetic procedures used for nanoparticles and nanorods. After injecting GeI_4 into preheated PdI_2 and TOP solution, the mixture was heated to 340 °C and kept the reaction for 30 min. Pd_2Ge nanowires were lengthened over several micrometers and entangled together (shown in Fig. 5(a and b)). Based on statistical analysis over 100 nanowires from the TEM and SEM images, the average diameter of nanowires was 15 ± 15 nm (shown in Fig. 5(c)). The detailed morphology of the Pd_2Ge nanowires was analyzed from HRTEM images (shown in Fig. 5(d and e)), and SAED patterns (shown in Fig. 5(f)) evidenced the growing plane of nanowires was (111), which corresponded to the peak at 37.6° in XRD database.

Morphology control of Pd_2Ge nanostructures

Observed from Fig. 1(a), several morphologies were obtained from the synthesis. Carried out with different mixtures of surfactants and various reaction times, several appropriate conditions for different morphologies of Pd_2Ge nanoproducts can be evaluated [30,31]. Shown in Fig. 6 and Fig. 7, we developed a series of experiments synthesizing Pd_2Ge. We firstly examined the surfactants using only OA, OLA and TOP

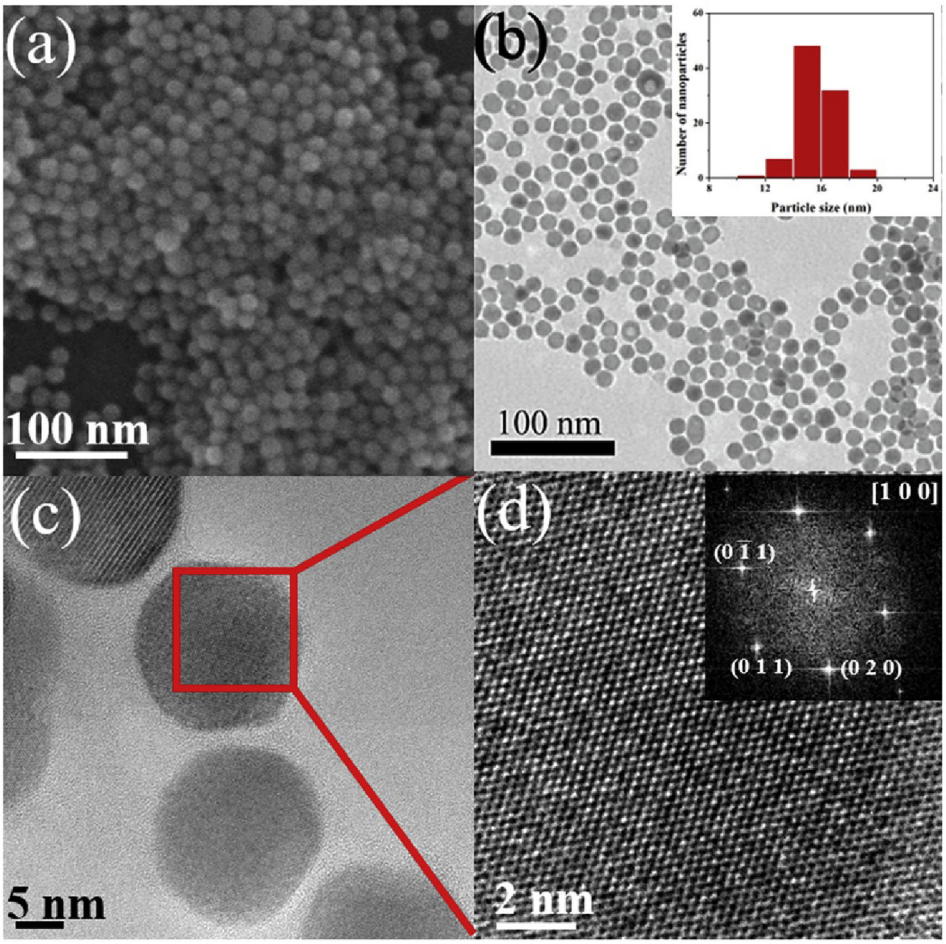

Fig. 3 – The (a) SEM image, (b) TEM image with statistics of Pd_2Ge nanoparticles diameter inserted, and (c-d) HRTEM images with the FFT pattern of Pd_2Ge nanoparticle inserted.

(shown in Fig. 6(a–l)). From Fig. 6(a),(d) and (g), the least TOP concentration (from Fig. 6 (d–f)) synthesized cubic-like nanorods, while the greater TOP concentration (from Fig. 6 (a–c)) synthesized thinner wire-like nanorods. However, when the surfactants mixture had the concentration of TOP much higher than that of OLA, which the result is shown in Fig. 6(a–c), the nanorods would aggregate.

On the other hand, reaction time seems to have no significant effect on the morphology (compared respectively among Fig. 6(a–c), Fig. 6(d–f), and Fig. 6(g and h)). However, when the reaction time extended from several hours (shown in Fig. 6(g and h)) to 24 h (shown in Fig. 6(i)), the synthesized nanorods would be thicker. Moreover, the higher concentration of OLA, the more nanorods were synthesized by comparing Fig. 6(j–l). Last, despite of OA, OLA and TOP, we also used other surfactants.

Fig. 6(m–o) shows the result of adding dodecylamine which the nanorods were successfully synthesized. Furthermore, when the reaction temperature changed from 260 °C (shown in Fig. 6(n)) to 300 °C (shown in Fig. 6(o)), the nanorods would be synthesized in more uniformed size and diameter. Comparing these three types of nanorods, the one that added dodecanethiol has two facets on the surface, while others only contained one facet on the surface. As a result, we used the former in the HER application.

In addition to adjusting the concentration of OLA and TOP in the surfactants mixture, the Fig. 7 illustrates the effect of the concentration of OA. Comparing Fig. 7 (b) with (d), the higher OA concentration synthesized longer nanorod-like products. Furthermore, by extending reaction time, the products were lengthened from nanorods to nanowires (comparing respectively among Fig. 7(a–c), Fig. 7(d–f)). However, nanoparticles were also appeared when the reaction time extended. Nonetheless, by comparing the results in Fig. 7(c, g, h) which are under higher OA concentration, we found out that the more TOP as a surfactant, fewer nanoparticles were synthesized. As a result, the reaction condition shown in Fig. 7(h) had a better morphology of nanowires comparing to the other conditions.

Different amounts of PdI_2 precursor and reaction condition were carried out to evaluate the appropriate condition for Pd_2Ge nanowires morphologies. In this series of experiments, we controlled three factors: the amount of PdI_2, the reaction temperature and the reaction. Comparing Fig. 8 (a) with (b), fewer particles were synthesized with higher reaction temperature. Next, we changed the reaction time from 1 h to 30

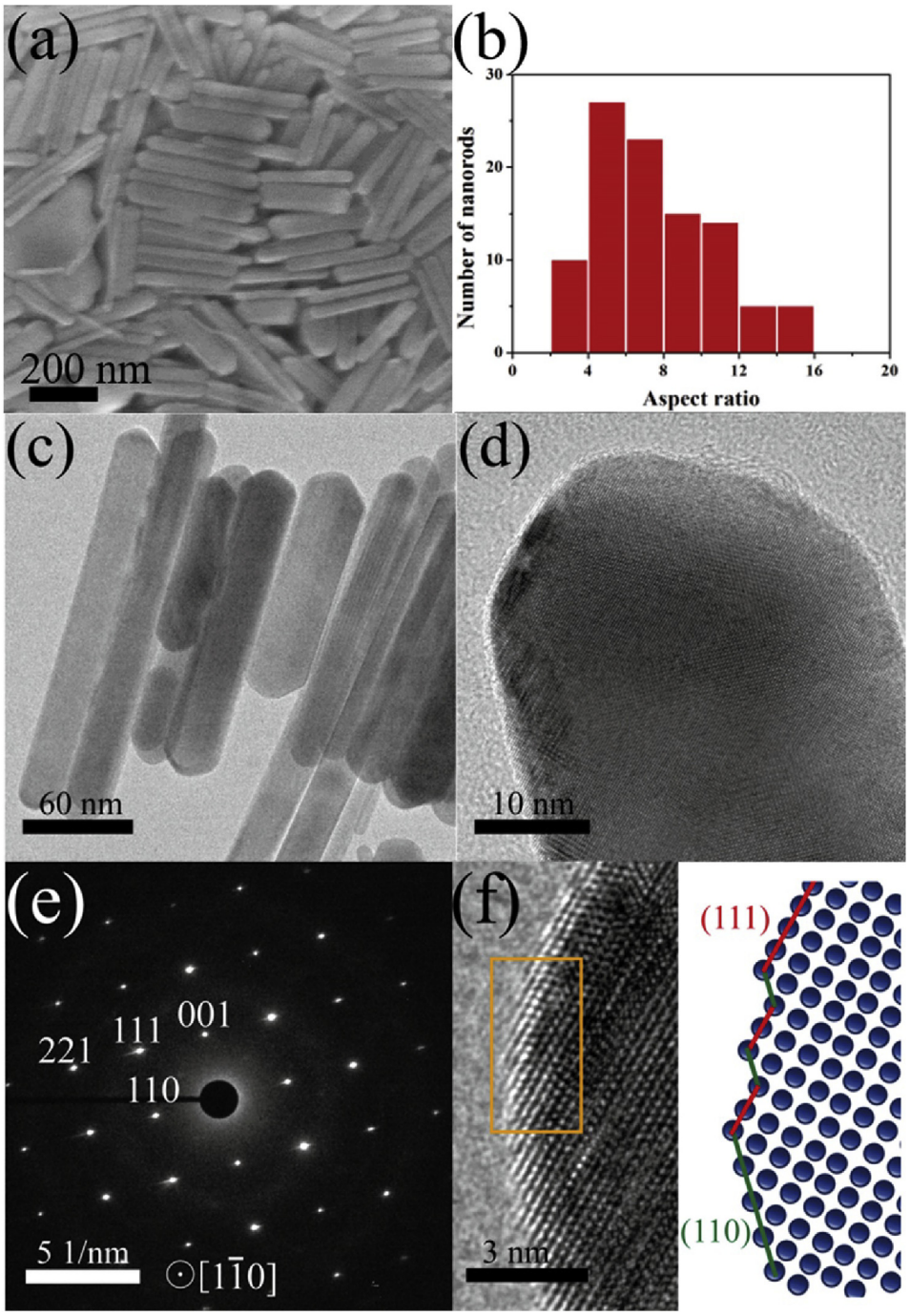

Fig. 4 – The (a) SEM image, (b) the statistics of Pd_2Ge nanorods aspect ratio, (c) TEM image, (d) HRTEM image, (e) the SAED pattern image and (f) is the HRTEM image and the simulation of two crystal facets surface.

and 15 min (shown Fig. 8(b–d)). However, there are no significant difference in the result between 1 h (shown in Fig. 8 (b)) and 30 min (shown in Fig. 8(c)) reactions, only the reaction of 15 min (shown in Fig. 8(d)) contained few nanowires and nanoparticles. As a result, we changed the amount of PdI_2 by double. Compared with the results between using PdI_2 38 mg (shown in Fig. 8(a–d)) and 79 mg (shown in Fig. 8(e, f)), the latter contained fewer nanoparticles. Furthermore, under the same reaction temperature (340 °C) and the same doubled amount of PdI_2, the result with 15 min' reaction time contained more nanoparticles, which might because of the growth is not complete. As a result, the best morphology of

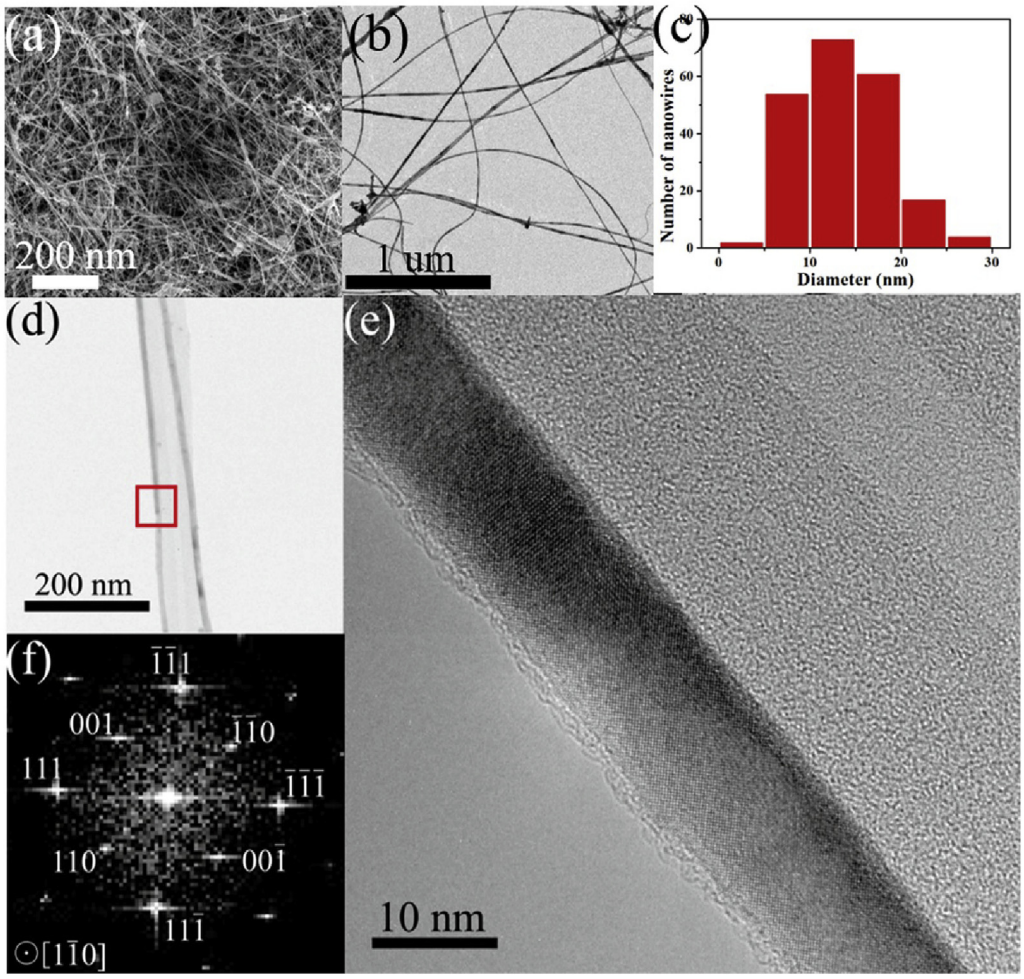

Fig. 5 – The (a) SEM image, (b, d) TEM image and (c) the statistics of Pd_2Ge nanowires diameter, (e) HRTEM image, (f) the FFT pattern image of Pd_2Ge nanowires.

Pd_2Ge nanowires were synthesized at the condition: using 79 mg of PdI_2, and setting the reaction temperature maintained at 340 °C for 30 min.

Hydrogen evolution reaction (HER)

Ge_2Pd Nanoparticles, nanorods and nanowires were further evaluated as catalysts in HER. The examination of the electrocatalytic activity of Pd_2Ge for HER was under a standard electrochemical arrangement. To that end, the working electrode was prepared by drop-coating the Pd_2Ge nanoink onto a rotating electrode, the mass loading was about 4 mg/cm^2 in 0.50 M. Shown in Fig. 9(a), the Pd_2Ge catalytic performances with three different morphologies (wires, rods, particles) in the hydrogen evolution reaction were in comparison. Also, we compared these performances with that of commercial Pd black. From Fig. 9(a), from the highest overpotential achieving a catalytic current density of 10 mA cm^{-2} to the lowest were listed: Pd_2Ge nanowires (−243 mV), commercial Pd black (−84 mV), Pd_2Ge nanoparticles (−63 mV) and Pd_2Ge nanorods (−17 mV) vs. reversible hydrogen potential (RHE). The performance between the commercial Pd black and Pd_2Ge nanoparticles were very similar. At the same time, the Pd_2Ge nanorods was the most active catalyst of HER compared with other morphologies and commercial Pd black. In previous studies, the catalytic activity depends on surface area, shape, and structure [32,33]. In order to improve the catalytic activity and stability, morphology controlling is one of the goals. Addition to enlarge the surface area, increasing the expose active sites approach has also attracted attention [34,35]. It is well accepted that increasing the exposed active sites can increasing the electro-catalytic activity, especially for nanomaterials [36,37]. Many research tried to tune the morphologies for controlling the active facets exposing to improve the catalytic performance. Herein, from the HRTEM image shown Fig. 4(f), the surface of nanorods actually contained two active facets while nanoparticles and nanowires only contained one active sites; as a result, nanorods would display more active character which required the less overpotential than other comparisons.

Moreover, Tafel plots, based on polarization, are shown in Fig. 9(b), and the curves are granted to explain specific underlying mechanism of HER. The linear region of Tafel plots were fitted with the Tafel equation ($\eta = b \log j + a$, where j is the current density), and Fig. 9(b) is the Tafel slope (which is b in the equation) in comparision. The Tafel slopes for Pd_2Ge

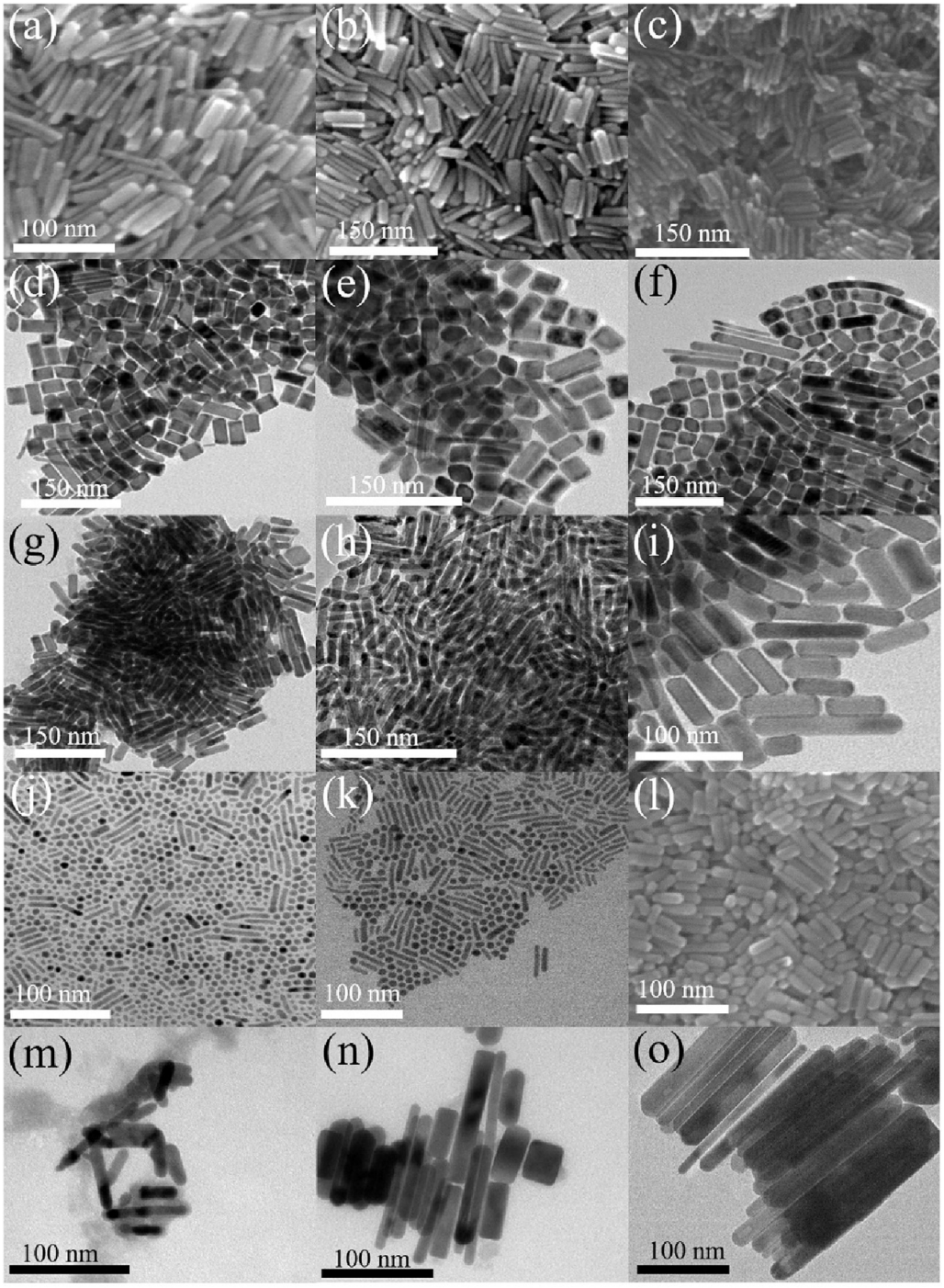

Fig. 6 – The SEM and TEM images of Pd_2Ge synthesized from different reaction conditions: (a) 11 ml OLA + 0.5 ml OA + 6 ml TOP at 260 °C with 0min, (b) 16 ml OLA + 0.5 ml OA +6 ml TOP at 260 °C with 30min, (c) 10 ml OLA +0.5 ml OA +6 ml TOP at 260 °C with 0min, (d) 16 ml OLA + 0.5 ml OA + 1 ml TOP at 260 °C with 0min, (e) 16 ml OLA + 0.5 ml OA + 1 ml TOP at 260 °C with 45min, (f) 16 ml OLA + 0.5 ml OA + 1 ml TOP at 260 °C with 120min, (g) 16 ml OLA + 0.5 ml OA + 3 ml TOP at 260 °C with 1hr, (h) 16 ml OLA + 0.5 ml OA + 3 ml TOP at 260 °C with 2hr, (i) 16 ml OLA + 0.5 ml OA + 3 ml TOP at 260 °C with 24hr, (j) 10 ml OLA +0.5 ml OA + 6 ml dodecanethiol at 300 °C with 0min, (k) 10 ml OLA +0.5 ml OA +6 ml dodecylamine at 260 °C with 45min, (l) 10 ml OLA +0.5 ml OA + 6 ml dodecanethiol at 260 °C with 45min.

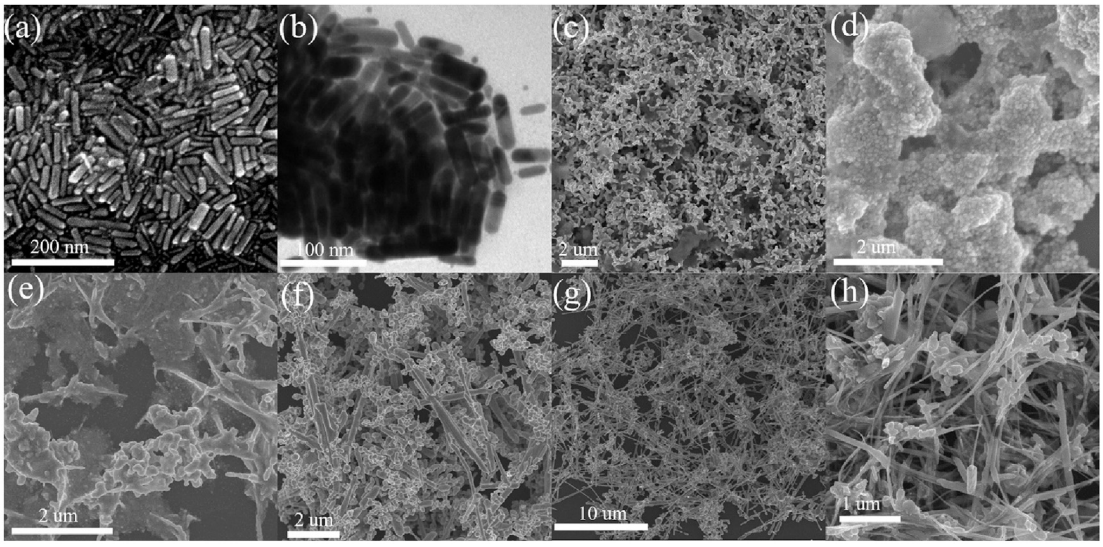

Fig. 7 – The SEM and TEM images of Pd_2Ge synthesized from different reaction conditions: (a) 16 ml OLA + 1 ml OA + 1 ml TOP at 320 °C with 40 min, (b) 16 ml OLA + 1.5 ml OA +1 ml TOP at 320 °C with 20 min, (c) 16 ml OLA +4.5 ml OA +1 ml TOP at 320 °C with 12 h, (d) 16 ml OLA + 1.5 ml OA + 3 ml TOP at 320 °C with 20 min, (e) 16 ml OLA + 1.5 ml OA + 3 ml TOP at 320 °C with 6 h, (f) 16 ml OLA + 1.5 ml OA + 3 ml TOP at 320 °C with 12 h, (g) 16 ml OLA + 4.5 ml OA + 3 ml TOP at 320 °C with 16hr, (h) 16 ml OLA + 4.5 ml OA + 6 ml TOP at 320 °C with 1hr.

nanowires, nanoparticles, nanorods and commercial Pd black were 143.4, 97.4, 75.1 and 74.9 mV dec^{-1}. In the hydrogen evolution reaction, the Volmer, the Heyrovsky and the Tafel step are the three fundamental mechanisms. The Volmer step is an imperative step since hydrogen intermediate is adsorbed in this step. Also, the previous research has reported the Heyrovsky and the Tafel step correlations in Tofel slopes [38,39]. The major difference between slops of the Heyrovsky and the Tafel step is the voltage, which is between-42 to −118 mV on the former slope and between −29 to ∞ (limiting current) mV on the latter slope. Therefore, considering the slope voltage, our catalyst might process under Volmer–Heyrovsky reaction since the rate determining step in HER mechanism is the electrochemical desorption. Furthermore, to have a better insight of the active surface area, based on the CV curves recorded by glassy carbon RDE deposited (Pd_2Ge nanoparticles and nanorods, which shown in Fig. S3 (a)-(b)), the electrochemically active surface area was also calculated (shown in supporting information). The ECSA of the catalyst was determined according to the following equation [40]: ECSA = Q/m*q, where m is the metal loading, and Q is the surface charge obtained from the CV area integrated, and we assumed the charge per real area of catalyst with monolayer adsorption of hydrogen is q = 210 (μC cm^{-2}) [41,42] which covered the Pd surface totally. By calculation, the ECSA result of the nanoparticles is 39.14 m^2/g and that of the nanorods is 103.6 m^2/g.

In addition, the stability of Pd_2Ge nanorods was examined in continuous cyclic voltammetric (CV) sweeps between −0.3 and + 0.1 V (vs. the reversible hydrogen electrode potential, RHE) (shown in Fig. S2 and Fig. 9). From Fig. 9(a), Pd_2Ge nanorods illustrated a retention with negligible changes in overpotential between initial cycle to 20,000-cycles CV sweeps. Thus, the overpotential at the 10 mA/cm^2 current densities after 20,000-cycle CV sweeps was still lower than the commercial Pd black. In addition, the long-term stability of Pd_2Ge nanorods catalyst was further examined with a high catalyst loading of ~4 mg/cm^2 on RDE by chronoamperometry measurement. The continuous HER process was performed at a constant overpotential of −0.5 V vs. RHE in 0.50 M H_2SO_4 for 48 h (Fig. 9(b)). Because of its two active sites on the surface, Pd_2Ge nanorods display extraordinary stability in the long-term test and is suggested as the prospect for implementing this new catalyst into realistic hydrogen evolution electrode. Shown in Fig. 9(b), the current density remained still after the 48-h operation, sufficiently shown the amazing stability and endurance of the Pd_2Ge nanorods as an electrocatalyst in acid media. Compared to the stability test of Pd_2Ge nanoparticles (shown in Fig. S2 (a, b)) and nanowires (shown in Fig. S2 (d)), the nanorods illustrate more stable with more CV swept cycles but smaller changes in overpotential. Still, the long-term test of nanoparticles displays impressive performance for successfully operating over 50 h without dramatic decrease in current density (the continuous HER process was performed at a constant overpotential of −0.45 V vs. RHE in 0.50 M H_2SO_4). The noise in the data is due to the electrode surface would contained the hydrogen bubble accumulation released during the hydrogen gas was continuous generated (inserted in Fig. S2 (b)).

In Table 1, the hydrogen evolution reaction activity and durability of this work and other Pd-based and Ge-based catalysts are compared and summarized. Comparing

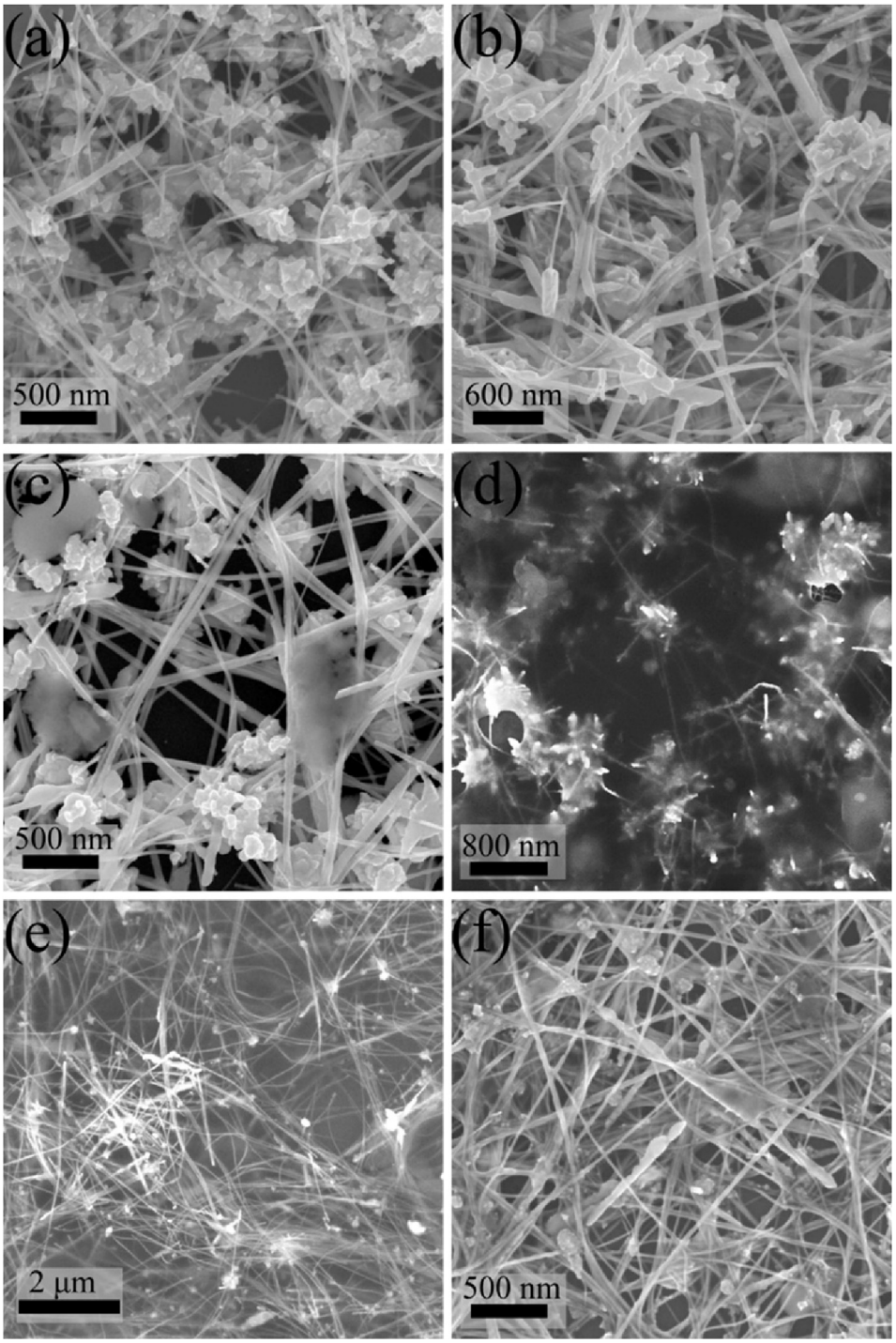

Fig. 8 – The SEM and TEM images of Pd_2Ge synthesized from different reaction conditions: (a) 38 mg PdI_2 in 16 ml OLA+6 ml TOP+4.75 ml OA at 320 °C with 1hr, (b) 38 mg PdI_2 in 16 ml OLA+6 ml TOP+4.75 ml OA at 340 °C with 1hr, (c) 38 mg PdI_2 in 16 ml OLA+6 ml TOP+4.75 ml OA at 340 °C with 30min, (d) 38 mg PdI_2 in 16 ml OLA+6 ml TOP+4.75 ml OA at 340 °C with 15min, (e) 79 mg PdI_2 in 16 ml OLA+6 ml TOP+4.75 ml OA at 340 °C with 30min, (f) 79 mg PdI_2 in 16 ml OLA+6 ml TOP+4.75 ml OA at 340 °C with 15min.

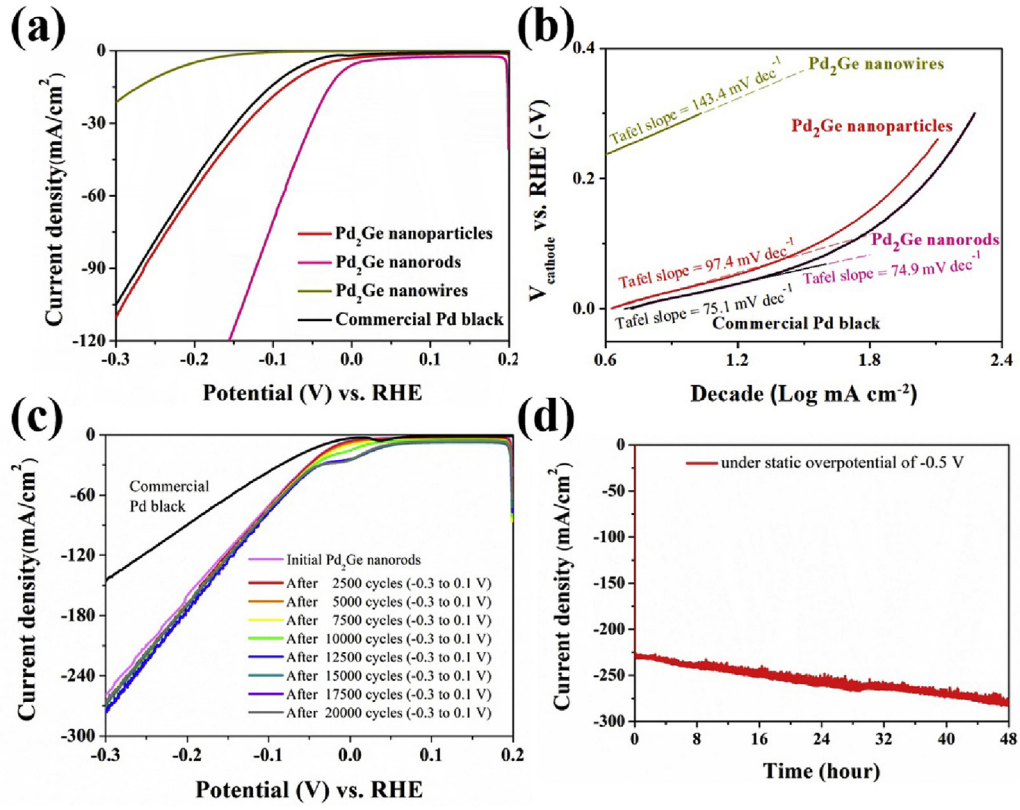

Fig. 9 – (a)Comparison of polarization data and (b) Tafel plots of polarization curves for commercial Pd and Pd_2Ge nanoparticles, nanorods and nanowires, (c) Polarization data for Pd_2Ge nanorods sample between −0.3 and 0.2V versus RHE, showing negligible current density loss even after 20,000 CV cycles. (d) Time dependence of current density under static overpotential of −0.5V

Table 1 – The comparison of HER performance among Pd-based and Ge-based electrode in 0.5 M H_2SO_4.

catalyst	electrolyte	overpotential vs. RHE (mV)	current density (mA/cm^2)	Long-term stability	CV sweeps	reference
Pd_2Ge nanorods	0.5 M H_2SO_4	17	10	48 h	20,000 cycles	This work
$GePt_3$ nanoparticles	0.5 M H_2SO_4	24	10	12 h	1000 cycles	[44]
Pd–Cu–S nanoporous	0.5 M H_2SO_4	58	10	48 h	3000 cycles	[45]
PdCu@Pd Nanocube	0.5 M H_2SO_4	68	10	48 h	5000 cycles	[46]
PdNP@N-CNT	0.5 M H_2SO_4	14 (48 based on the reference calculation)	1	10,000 s	–	[47]
3D-Pd/rGO	0.5 M H_2SO_4	120	10	14,000 s	1000 cycles	[48]
PdMnCo/NC	0.5 M H_2SO_4	38	10	80 h	–	[43]
rGO-$Au_{48}Pd_{52}$	0.5 M H_2SO_4	280	10	15hr	–	[49]

catalysts are mainly Pd-based catalysts, such as Pd–Cu–S ternary material, PdCu@Pd nanocube, Pd Nanoparticles, Pd/rGO, PdMnCo/NC, and rGO-$Au_{48}Pd_{52}$. Among all the catalysts, our as-prepared Pd2Ge nanorods have the lowest overpotential, indicating our nanorods obtain higher catalytic activity comparing to other works. Even though PdMnCo/NC [43] demonstrated better stability with continuing operating 80 h, our as-prepared catalyst has second long-term stability (40 h) with the most active electro-catalyst at 10 mA/cm^2.

For further analysis of the electro-catalytic active surface of different morphologies, electric impedance spectroscopy (EIS) was carried out (shown in Fig. 10). The EIS data are fitted by electrical equivalent circuit which is the inserted diagram in the

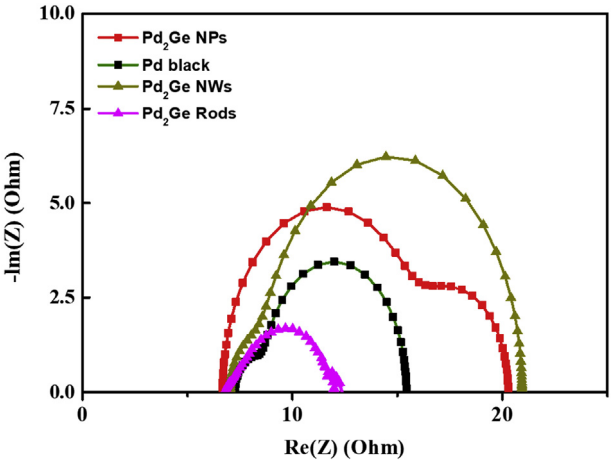

Fig. 10 – Comparison of EIS Nyquist results at −0.12 V overpotential (vs. RHE) with a scanning frequency of 105–0.01 Hz (Pd_2Ge nanoparticles, Pd black, Pd_2Ge nanowires and Pd_2Ge nanorods). Inserted is the equivalent circuit diagram; C2 and C3 are the two constant phases, and the R1 represents the series resistance, R2 is the polarization resistance, R3 stands for the over potential dependent charge transfer coefficient.

Fig. 10 [50,51]. The obtain EIS results demonstrated the proportion of the reaction resistances, which related to the diameter of the semicircle. In other words, the larger the diameter of the semicircle, the higher reaction resistance of the material has. From the results, the Pd_2Ge nanorods have display smallest diameter comparing to others, indicating the nanorods obtain fewer reaction resistance and have faster electron transferring pathway. Furthermore, the diameter sequence also corresponds to the overpotential results, suggesting the nanorods have the higher electro-catalytic activity in the HER.

Conclusions

Various morphologies of Pd_2Ge via changing the mixture surfactants were obtained in one-pot solution method. Nanoparticles, cubic-like nanorods, wire-like nanorods, two crystal facets of nanorods and nanowires were obtained by changing the proportion of the surfactants, similar temperature and reaction time. An investigation and comparisons of these Pd_2Ge nanostructures are implemented as electrocatalysts for HER, indicating elecrocatalytic performance is shape-dependent. The nanorods have not only shown an outstanding activity which obtained the lowest overpotential among than the commercial Pd black and the other nanostructures, but also displayed amazing endurance with the catalytic performance remained still after 20,000 CV sweep and under a static overpotential of −0.5 V vs. RHE for 48 h. Compared to previous result, the synthesized Pd2Ge nanorods illustrated both high electro-catalytic activity and stability. As a result, Pd_2Ge nanorods is suggested the prospect for implementing the shape-dependent approach into improving the realistic performance of hydrogen evolution electrodes.

Acknowledgment

We acknowledge the financial support by the Ministry of Science and Technology through the grants of MOST 106-2221-E-007-081-MY3, 106-2628-E-007-005-MY3, and 103-2221-E-007-089-MY3, and MOST 106-2622-8-007-017, and by National Tsing Hua University through the grant of 107Q2708E1.

Appendix A. Supplementary data

Supplementary data to this article can be found online at https://doi.org/10.1016/j.ijhydene.2019.03.062.

REFERENCES

[1] Cao ZM, Li HQ, Zhan CY, Zhang JW, Wang W, Xu BB, et al. Monocrystalline platinum-nickel branched nanocages with enhanced catalytic performance towards the hydrogen evolution reaction. Nanoscale 2018;10:5072–7.
[2] Wang PT, Zhang X, Zhang J, Wan S, Guo SJ, Lu G, et al. Precise tuning in platinum-nickel/nickel sulfide interface nanowires for synergistic hydrogen evolution catalysis. Nat Commun 2017;8.
[3] Cao ZM, Chen QL, Zhang JW, Li HQ, Jiang YQ, Shen SY, et al. Platinum-nickel alloy excavated nano-multipods with hexagonal close-packed structure and superior activity towards hydrogen evolution reaction. Nat Commun 2017;8.
[4] Kye J, Shin M, Lim B, Jang JW, Oh I, Hwang S. Platinum monolayer electrocatalyst on gold nanostructures on silicon for photoelectrochemical hydrogen evolution. ACS Nano 2013;7:6017–23.
[5] Wu JJ, Lu SL, Ge DH, Zhang LZ, Chen W, Gu HW. Photocatalytic properties of Pd/TiO_2 nanosheets for hydrogen evolution from water splitting. RSC Adv 2016;6:67502–8.
[6] Rasouli H, Tabaian SH, Rezaei M. Galvanic replacement of electrodeposited nickel by palladium and investigation of the electrocatalytic activity of synthesized Pd/(Ni) for hydrogen evolution and formic acid oxidation. RSC Adv 2016;6:22500–10.
[7] Sarkar S, Jana R, Waghmare UV, Kuppan B, Sampath S, Peter SC. Ordered Pd2Ge intermetallic nanoparticles as highly efficient and robust catalyst for ethanol oxidation. Chem Mater 2015;27:7459–67.
[8] Bodnar Z, Mallat T, Baiker A. Reactant induced restructuring and corrosion of germanium-palladium catalysts during hydrogenation reactions. Catal Lett 1994;26:61–70.
[9] Reddy NP, Yamashita H, Tanaka M. Platinum- or palladium-catalysed ring-opening homo- and co-polymerization of silicon- and germanium-bridged [1]ferrocenophanes. J Chem Soc, Chem Commun 1995:2263–4.
[10] Bodnar Z, Mallat T, Baiker A. Bulk alloy formation during Ge adsorption onto a Pd-powder catalyst. J Electroanal Chem 1993;358:327–31.

[11] Gootzen JFE, Lefferts L, van Veen JAR. Electrocatalytic nitrate reduction on palladium based catalysts activated with germanium. Appl Catal, A 1999;188:127–36.
[12] Aduriz HR, Bodnariuk P, Coq B, Figueras F. Alumina-supported bimetallics of palladium alloyed with germanium, tin, lead, or antimony from organometallic precursors: I. Preparation and characterization. J Catal 1989;119:97–107.
[13] Okamoto H. The Ge-Pd system (germanium-palladium). J phase equilib 1992;13:410–3.
[14] Galvagno S2, Poltarzewski, Donato A, Neri G, Pietropaolo R. J Chem Soc, Chem Commun 1986:1729.
[15] Sarkar S, Jana R, Suchitra, Waghmare UV, Kuppan B, Sampath S, et al. Ordered Pd2Ge intermetallic nanoparticles as highly efficient and robust catalyst for ethanol oxidation. Chem Mater 2015;27:7459–67.
[16] Segura RA, Tello A, Haberle P. Synthesis of carbon nanotubes, nanofibers and encapsulated nanoparticles by decomposition of acetylene on Ge modified Pd catalysts. Phys Status Solidi 2007;204:1781–5.
[17] Behrens S. Preparation of functional magnetic nanocomposites and hybrid materials: recent progress and future directions. Nanoscale 2011;3:877–92.
[18] Jain PK, Huang X, El-Sayed IH, El-Sayed MA. Noble metals on the nanoscale: optical and photothermal properties and some applications in imaging, sensing, biology, and medicine. Acc Chem Res 2008;41:1578–86.
[19] Wang C, Daimon H, Onodera T, Koda T, Sun SH. A general approach to the size- and shape-controlled synthesis of platinum nanoparticles and their catalytic reduction of oxygen. Angew Chem Int Ed 2008;47:3588–91.
[20] Zhang ZP, Marson RL, Ge ZS, Glotzer SC, Ma PX. Simultaneous nano- and microscale control of nanofibrous microspheres self-assembled from star-shaped polymers. Adv Mater 2015;27:3947–52.
[21] Talapin DV, Lee J-S, Kovalenko MV, Shevchenko EV. Prospects of colloidal nanocrystals for electronic and optoelectronic applications. Chem Rev 2009;110:389–458.
[22] Park J, Joo J, Kwon SG, Jang Y, Hyeon T. Synthesis of monodisperse spherical nanocrystals. Angew Chem Int Ed 2007;46:4630–60.
[23] Tao AR, Habas S, Yang PD. Shape control of colloidal metal nanocrystals. Small 2008;4:310–25.
[24] Yang PD. Shape control of colloidal metal nanocrystals. Abstr Pap Am Chem Soc 2009;237.
[25] Biacchi AJ, Schaak RE. The solvent matters: kinetic versus thermodynamic shape control in the polyol synthesis of rhodium nanoparticles. ACS Nano 2011;5:8089–99.
[26] Lu C-L, Prasad KS, Wu H-L, Ho J-aA, Huang MH. Au nanocube-directed fabrication of Au– Pd core– shell nanocrystals with tetrahexahedral, concave octahedral, and octahedral structures and their electrocatalytic activity. J Am Chem Soc 2010;132:14546–53.
[27] Cui C, Gan L, Heggen M, Rudi S, Strasser P. Compositional segregation in shaped Pt alloy nanoparticles and their structural behaviour during electrocatalysis. Nat Mater 2013;12:765.
[28] Shao M, Yu T, Odell JH, Jin M, Xia Y. Structural dependence of oxygen reduction reaction on palladium nanocrystals. Chem Commun 2011;47:6566–8.
[29] Huang MH, Lin PH. Shape-controlled synthesis of polyhedral nanocrystals and their facet-dependent properties. Adv Funct Mater 2012;22:14–24.
[30] Wu J, Gross A, Yang H. Shape and composition-controlled platinum alloy nanocrystals using carbon monoxide as reducing agent. Nano Lett 2011;11:798–802.
[31] Somorjai GA, Blakely D. Mechanism of catalysis of hydrocarbon reactions by platinum surfaces. Nature 1975;258:580.
[32] Andreiadis ES, Jacques P-A, Tran PD, Leyris A, Chavarot-Kerlidou M, Jousselme B, et al. Molecular engineering of a cobalt-based electrocatalytic nanomaterial for H 2 evolution under fully aqueous conditions. Nat Chem 2013;5:48.
[33] Kumar SS, Selvakumar K, Thangamuthu R, Selvi AK, Ravichandran S, Sozhan G, et al. Hydrothermal assisted morphology designed MoS2 material as alternative cathode catalyst for PEM electrolyser application. Int J Hydrogen Energy 2016;41:13331–40.
[34] Kibsgaard J, Chen Z, Reinecke BN, Jaramillo TF. Engineering the surface structure of MoS 2 to preferentially expose active edge sites for electrocatalysis. Nat Mater 2012;11:963.
[35] Yu H, Yu X, Chen Y, Zhang S, Gao P, Li C. A strategy to synergistically increase the number of active edge sites and the conductivity of MoS 2 nanosheets for hydrogen evolution. Nanoscale 2015;7:8731–8.
[36] Ni B, Wang X. Face the edges: catalytic active sites of nanomaterials. Adv Sci 2015;2:1500085.
[37] Yang TT, Saidi WA. Tuning the hydrogen evolution activity of β-Mo 2 C nanoparticles via control of their growth conditions. Nanoscale 2017;9:3252–60.
[38] Tang Q, Jiang D-e. Mechanism of hydrogen evolution reaction on 1t-MoS2 from first principles. ACS Catal 2016;6:4953–61.
[39] Videa M, Crespo D, Casillas G, Zavala G. Electrodeposition of nickel-molybdenum nanoparticles for their use as electrocatalyst for the hydrogen evolution reaction. J New Mater Electrochem Syst 2010;13:239–44.
[40] Du Y, Ni K, Zhai Q, Yun Y, Xu Y, Sheng H, et al. Facile air oxidative induced dealloying of hierarchical branched PtCu nanodendrites with enhanced activity for hydrogen evolution. Appl Catal, A 2018;557:72–8.
[41] Martin M, Lasia A. Study of the hydrogen absorption in Pd in alkaline solution. Electrochim Acta 2008;53:6317–22.
[42] Shi J-J, Zhu J-J. Sonoelectrochemical fabrication of Pd-graphene nanocomposite and its application in the determination of chlorophenols. Electrochim Acta 2011;56:6008–13.
[43] Zhang R, Sun Z, Feng R, Lin Z, Liu H, Li M, et al. Rapid adsorption enables interface engineering of PdMnCo alloy/nitrogen-doped carbon as highly efficient electrocatalysts for hydrogen evolution reaction. ACS Appl Mater Inter 2017;9:38419–27.
[44] Lim S-C, Hsiao M-C, Lu M-D, Tung Y-L, Tuan H-Y. Synthesis of germanium–platinum nanoparticles as high-performance catalysts for spray-deposited large-area dye-sensitized solar cells (DSSC) and the hydrogen evolution reaction (HER). Nanoscale 2018;10:16657–66.
[45] Xu W, Zhu S, Liang Y, Cui Z, Yang X, Inoue A, et al. A highly efficient electrocatalyst based on amorphous Pd–Cu–S material for hydrogen evolution reaction. J Mater Chem 2017;5:18793–800.
[46] Li J, Li F, Guo S-X, Zhang J, Ma J. PdCu@ Pd nanocube with Pt-like activity for hydrogen evolution reaction. ACS Appl Mater Inter 2017;9:8151–60.
[47] Zhou S, Chen X, Yu P, Gao F, Mao L. Nitrogen-doped carbon nanotubes as an excellent substrate for electroless deposition of Pd nanoparticles with a high efficiency toward the hydrogen evolution reaction. Electrochem Commun 2018;90:91–5.
[48] Ensafi AA, Heydari-Soureshjani E, Rezaei B. Three-dimensional graphene promoted by palladium nanoparticles, an efficient electrocatalyst for energy production and storage. Int J Hydrogen Energy 2018;43:9652–62.
[49] Cardoso J, Amaral L, Metin Ö, Cardoso D, Sevim M, Sener T, et al. Reduced graphene oxide assembled Pd-based

nanoalloys for hydrogen evolution reaction. Int J Hydrogen Energy 2017;42:3916–25.

[50] Bhowmik T, Kundu MK, Barman S. Palladium nanoparticle–graphitic carbon nitride porous synergistic catalyst for hydrogen evolution/oxidation reactions over a broad range of pH and correlation of its catalytic activity with measured hydrogen binding energy. ACS Catal 2016;6:1929–41.

[51] Ge Y, Wu J, Xu X, Ye M, Shen J. Facile synthesis of $CoNi_2S_4$ and $CuCo_2S_4$ with different morphologies as prominent catalysts for hydrogen evolution reaction. Int J Hydrogen Energy 2016;41:19847–54.